Journal of Biomechanics

Considerations for analysis of endothelial shear stress and strain in FSI models of atherosclerosis

--Manuscript Draft--

Manuscript Number:	BM-D-20-01443R1
Article Type:	Full Length Article (max 3500 words)
Keywords:	Murine carotid artery; wall shear stress; Endothelial Strain metrics; Histology co-registration; fluid-structure interaction; computational fluid dynamics
Corresponding Author:	Rob Krams Queen Mary University of London London, UNITED KINGDOM
First Author:	Rob Krams
Order of Authors:	Rob Krams
	Miten B. Patel
	Fotios Savvopoulos
	Caleb C. Berggren
	Lydia Aslanidou
	Lucas H. Timmins
	Ranil de Silva
	Ryan M. Pedrigi
Abstract:	Atherosclerosis is a lipid driven chronic inflammatory disease that is characterized by the formation of plaques at predilection sites. These predilection sites (side branches, curved segments, and bifurcations) have often been associated with disturbed shear stress profiles. However, in addition to shear stress, endothelial cells also experience artery wall strain that could contribute to atherosclerosis progression. Herein, we describe a method to accurately obtain these shear stress and strain profiles. We developed a fluid-structure interaction (FSI) framework for modelling arteries within a commercially available package (Abaqus, version 6.12) that included known prestresses (circumferential, axial and pressure associated). In addition, we co-registered 3D histology to a micro-CT-derived 3D reconstruction of an atherosclerotic carotid artery from a cholesterol-fed ApoE-/- mouse to include the spatial distribution of lipids within a subject-specific model. The FSI model also incorporated a nonlinear hyperelastic material model with regionally-varying properties that distinguished between healthy vessel wall and plaque. FSI predicted a lower shear stress than CFD (~-12%), but further decreases in plaque regions with softer properties (~-24%) were dependent on the approach used to implement the prestresses in the artery wall. When implemented with our new hybrid approach (zero prestresses in regions of lipid deposition), there was significant heterogeneity in endothelial shear stress in the atherosclerotic artery due to variations in stiffness and, in turn, wall strain. In conclusion, when obtaining endothelial shear stress and strain in diseased arteries, a careful consideration of prestresses is necessary. This paper offers a way to implement them.

Queen Mary University of London
Mile End Road, London E1 4NS
Telephone: +44(0)20 7882 5555
Fax: +44(0)20 89831007

Professor Rob Krams
Chair in Molecular Bioengineering
Room 3.15
School of Engineering and Material Science
Mile End
London, E! 4NS

27/11/2020

Dear Sir/Madam

I would like to *re*-submit the manuscript: "Considerations for analysis of endothelial shear stress and strain in FSI models of atherosclerosis" for a full-publication. We thank the editor for allowing us to submit a full paper after sending our manuscript to be evaluated as a short technical report.

This manuscript is not send to any other journal, and all co-authors are aware of this publication and have been involved in the paper. We hope the content of this short communication is of sufficient quality to warrant publication in your journal.

Yours Sincerely,

With Regards,

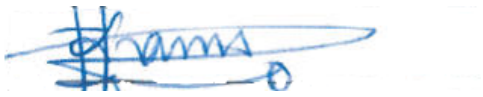

Dr. Rob Krams

Professor of Molecular Bioengineering

Queen Mary University London

London

Reviewer comments:

Reviewer #1: This manuscript reports the results of an extensive investigation on the estimation of shear stress and strain in the carotid artery of a mouse that developed vascular diseases. The experimental technique and the numerical analysis have been usefully planed and conducted. While the methods used have been carefully selected and validated or commented, there are however, very few experimental data to support the hypothesis that endothelial strain over atherosclerotic plaque is involved in the mechanism of disease progression and plaque vulnerability. I have the following comments for Authors' consideration.

1) The use of a single vessel from only one animal is very limited to demonstrate convincingly the relation between EC shear stress, strain and atherosclerotic changes. The main comparisons and conclusions are based on the observation reported in Figure 5, that are not even numerically reported. In my opinion, the data presented do not support the conclusions of this manuscript that shear stress and strain vector angle changes over the plaque tissue, and in addition that cyclic strain on EC increased over the plaque region. While these hypothesis is interesting and challenging, it needs more extensive experimental evaluation.

Reply: The primary purpose of this paper is to report the development of an FSI model of a murine atherosclerotic artery to examine the effect of differences in assumptions on the predictions of shear stress and wall strain. We feel that data from a representative mouse is sufficient towards this end. We have rewritten the Results and Discussion sections to more clearly bring out this point and have redone many of the figures, including the addition of histograms, to better quantify the results. We agree with the reviewer that more mice are needed to draw conclusions about changes in endothelial strain in atherosclerosis and their effect on plaque progression. We originally introduced new strain metrics and examined their change in plaque regions to motivate the need for FSI modelling. Given the criticism, we have now removed these metrics and associated results from the paper.

2) In line with previous comment, the mechanisms responsible for atherosclerotic plaque initiation and progress may be very different in mouse and in humans. I would be hesitant to

extend the observation in a mouse model to the mechanisms responsible for the human disease.

Reply: As stated above, we are exclusively focused on the technical aspects of developing an accurate FSI model. We demonstrate that the Hybrid Model allows for realistic predictions of strain and TAWSS within regions of lipid deposition (in contrast to the nominal and histology models) by showing an increase in strain in these softer regions that leads to a larger decrease in TAWSS compared to that predicted by CFD. This was not seen in softer regions of the artery in the Histology Model, despite the inclusion of lipid properties (the nominal model does not have altered properties in plaque regions). To further support our novel hybrid approach, we have now added data where stiffness in the lipid regions was arbitrarily *increased* by 10-fold, which significantly lowered the predicted strain and lessened the change in TAWSS. Thus, both data sets (soft plaques and stiffened plaques) indicate that our proposed framework for developing FSI models of diseased, murine arteries is realistic.

3) Despite these criticisms, the methods used is valuable and show interesting features of the experimental approach and the numerical analysis. I wonder whether the manuscript should be focussed completely on a technical report, with the aim to develop and validate a new approach to investigate vessel wall mechanical strain and wall shear stress. This type of approach is rather innovative in order to shed more light on the effects of local hemodynamic conditions on atherosclerotic vascular changes. Actually, the consideration of only WSS metrics does not allow to explain completely these phenomena.

Reply: We thank the reviewer for recognising that this paper introduces extensive innovations to the CFD/FSI field. As stated above, the purpose of this paper is to evaluate different assumptions related to the development of an FSI model of an atherosclerotic artery, with a particular focus on how to incorporate prestresses into the model. We are not attempting to report how mechanical metrics from FSI correlate to or predict plaque progression. Originally, we submitted this paper to this journal as a Short Communication. However, space restrictions did not allow us to fully describe all details of the novel computational techniques introduced in this study and their relevance to atherosclerosis

within the context of other computational studies. Consequently, the editor asked us to extend the technical paper to a full paper. Because the emphasis of the full paper remains technical, we attempted to avoid strong statements and/or definite conclusions on the role of FSI derived metrics in Atherosclerosis. Given the concern of the reviewer, we have made additional changes to make clear that this paper presents findings that could aid in the development of accurate FSI models and further work is needed to assess how mechanical metrics from such models better predict atherosclerosis.

4) *The main comparisons and conclusions are based on the observation reported in Figure 5, that are not even numerically reported*

Reply: We thank the reviewer for raising this issue and agree that better quantification of the results would improve clarity. As such, we have now redone most of the figures of the paper to improve the primary messages around differences from CFD and the best way to incorporate prestresses into an FSI model, and have included several histograms to quantify the results.

5) In line with previous comment, the mechanisms responsible for atherosclerotic plaque initiation and progress may be very different in mouse and in humans. I would be hesitant to extend the observation in a mouse model to the mechanisms responsible for the human disease

Reply: This is an important point. While the animal model has been used in numerous studies, it is now accepted that the short, intense period of cholesterol feeding leads to lipid-rich and soft plaques. In patients, lipid-rich plaques often occur in conjunction with fibrous plaques, so there are some similarities. However, as stated above (Q1 and Q2), the purpose of this paper is to report a new framework for the development of FSI models of murine arteries with a particular emphasis on differences from CFD and how to incorporate prestresses into the model to achieve realistic predictions of relevant mechanical quantities. We feel that the reported FSI framework is translatable to the development of models of arteries from other species, including humans.

Reviewer #2: This is a thorough, well written paper which I have read with interest. In reviewing this manuscript by Patel and arounds, I interpreted my role as a Reviewer who intervenes at the second step of the review process. For this reason, my review was mainly focused on evaluating how the Authors have addressed Reviewers concerns. In this optics, my comment is that the Authors have almost satisfactorily addresses most of the concerns raised by previous Reviewers.
My only comments are that I would have preferred to read:

(1) a more critical discussion about the use of the animal model adopted here. Is really the mice cuff model representative of the human atherosclerosis "biomechanical machinery"?

Reply: Please see response above (R1, Q5).

(2) a more clear take-home-message from the Authors. Based on their findings and on the idealizations/assumptions introduced, can the Authors conclude that their FSI-based approach is necessary to identify low/high TAWSS regions at the luminal surface?

Reply: We thank the reviewer for this excellent suggestion. We agree that the primary message of the paper could be articulated more clearly. We have largely rewritten the Results and Discussion sections to emphasize our primary technical points about FSI model development, including redoing most of the figures with improved quantification. Our results demonstrate substantial differences in the prediction of TAWSS in FSI versus CFD, wherein the Hybrid FSI Model showed a median difference from CFD in the regions of lipid deposition of -23.8%. Since this difference is greater than that for the non-diseased regions (-11.4%), it indicates that FSI modelling with altered properties in plaque regions will change the prediction of shear stress and related metrics. Presumably, this will lead to improved ability of the FSI models to predict plaque progression, but a larger study with more mice will be needed to confirm this conclusion. We have now added this point to the Discussion.

Considerations for analysis of endothelial shear stress and strain in FSI models of atherosclerosis

Miten Patel[2,7 *], Fotios Savvopoulos[1,2,7*], Caleb C. Berggren[3], Lydia Aslanidou[4], Lucas H. Timmins[5,6], Ranil de Silva[2], Ryan M. Pedrigi[3], and Rob Krams[7]

[1]Bioengineering and [2]NHLI, Imperial College, UK, [3]Mechanical & Materials Engineering, University of Nebraska-Lincoln, USA, [4]Institute of Bioengineering, Ecole Polytechnique Fédérale de Lausanne, Switzerland, [5]Biomedical Engineering, University of Utah, USA, [6]Scientific Computing and Imaging Institute, University of Utah, [7]Queen Mary University, School for Material Sciences and Engineering, UK, * shared first author

Correspondence:

Rob Krams, M.D., Ph.D.
Head of the Division of Bioengineering
Scientific Director, CVDHub, Bart's Heart Centre
Chair in Molecular Bioengineering

School of Engineering and Material Sciences
Queen Mary University London
Mile End, E1 4NS.

Email: r.krams@qmul.ac.uk
Tel: +442078827940
Tel: +447972413211

Keywords: murine carotid artery, atherosclerotic plaques, wall shear stress, endothelial strain, mechanical modelling, fluid-structure interaction, computational fluid dynamics, residual stress, Backward Incremental method

Word Count: 3800

Abstract

Atherosclerosis is a lipid driven chronic inflammatory disease that is characterized by the formation of plaques at predilection sites. These predilection sites (side branches, curved segments, and bifurcations) have often been associated with disturbed shear stress profiles. However, in addition to shear stress, endothelial cells also experience artery wall strain that could contribute to atherosclerosis progression. Herein, we describe a method to accurately obtain these shear stress and strain profiles.

We developed a fluid-structure interaction (FSI) framework for modelling arteries within a commercially available package (Abaqus, version 6.12) that included known prestresses (circumferential, axial and pressure associated). In addition, we co-registered 3D histology to a micro-CT-derived 3D reconstruction of an atherosclerotic carotid artery from a cholesterol-fed ApoE$^{-/-}$ mouse to include the spatial distribution of lipids within a subject-specific model. The FSI model also incorporated a nonlinear hyperelastic material model with regionally-varying properties that distinguished between healthy vessel wall and plaque.

FSI predicted a lower shear stress than CFD (~-12%), but further decreases in plaque regions with softer properties (~-24%) were dependent on the approach used to implement the prestresses in the artery wall. When implemented with our new hybrid approach (zero prestresses in regions of lipid deposition), there was significant heterogeneity in endothelial shear stress in the atherosclerotic artery due to variations in stiffness and, in turn, wall strain.

In conclusion, when obtaining endothelial shear stress and strain in diseased arteries, a careful consideration of prestresses is necessary. This paper offers a way to implement them.

1. Introduction

Atherosclerosis is a chronic, lipid-driven inflammatory disease that progresses from simple to advanced plaques composed of a soft, lipid-rich necrotic core covered by a thin cap. Although it is a multifactorial disease, plaques tend to localize in regions of the vasculature with high curvature, side branches or bifurcations. The endothelium of these vessel regions often experiences disturbed blood flow and decades of research have demonstrated a correlation between arterial regions and locally disturbed flow and atherosclerosis (Morbiducci et al., 2016; Yurdagul et al., 2016). Recent studies, including ours, have demonstrated a causal, not just correlative, relationship between disturbed flow and the development of advanced atherosclerotic plaques (Cheng et al., 2006; Pedrigi et al., 2016; Pedrigi et al., 2015).

While blood flow-derived shear stress on the endothelium has been used in research for the development of metrics to predict atherosclerosis progression and plaque composition, the performance of these metrics in patients is still debated (Stone et al., 2018). In addition to time-dependent shear stress, endothelial cells also experience pulsatile, blood pressure-induced artery wall stress and strain (Kobielarz et al., 2020; Pedrigi et al., 2014; Pedrigi et al., 2017). The role of endothelial strain in atherogenesis has been far less studied than shear stress, but previous work by us and others have shown that disturbed strain profiles activate pro-atherogenic pathways similar to shear stress (Chester et al., 2014; Kwak et al., 2014; Liu et al., 2013; Pedrigi et al., 2017; Peters et al., 2015). The accumulation of lipids strongly enhances the heterogeneity of the mechanical environment in the plaque-affected areas. Thus, use of modelling techniques that allow elucidation of the highly heterogeneous mechanical environment of atherosclerotic plaques with stiff collagen-rich areas juxtaposed to soft lipid-rich zones (Alberts-Grill et al., 2013; Chistiakov et al., 2015; Krams et al., 2005; Tian et al., 2014; Trogan et al., 2002), may shed light on the still largely unknown mechanobiological effects of complex strain fields on endothelial cells and improve metrics seeking to predict atherosclerosis progression.

Accordingly, this paper describes the development of a fluid-structure interaction (FSI) model from *in vivo* micro-CT imaging of the carotid arteries of an ApoE$^{-/-}$ mouse that incorporates most mechanical complexities of the blood and diseased artery wall. These complexities include: circumferential residual stress, axial prestress, circumferential prestress due to diastolic blood pressure (Fung, 1991; Taber, 1995), and a nonlinear hyperelastic material model that has regionally-varying stiffness determined by co-registered histology to discriminate between healthy vessel wall and regions of lipid deposition in atherosclerotic plaques. In line with previous reports, we demonstrate that a distensible artery wall in FSI causes a substantial reduction to the predicted wall shear stress compared to the use of a rigid wall in CFD (Trachet et al., 2015). In addition, there was a further reduction in wall shear stress within the plaque regions which was dependent on the approach used to implement the residual stress and prestresses in the artery wall.

2. Methods

2.1 Animals, surgery, imaging, histology and mesh generation

The model geometry, inlet velocity boundary condition and co-registered 3D histology used to develop the FSI model were based upon a subset (1 female ApoE$^{-/-}$ mouse) of the data available from a prior study (Pedrigi et al., 2016) (**Fig. S1**, **Appendix A**). This mouse, aged 11 weeks, was placed on a high-fat diet and two weeks later instrumented with a blood flow-modifying tapering cuff around the left carotid artery, as previously described (Cheng et al., 2006; Pedrigi et al., 2016). The right carotid artery served as an un-instrumented control. The mouse was injected with a metal-based nanoparticle contrast agent and scanned using an ultra-high precision micro-computed tomography (micro-CT) system (isotropic resolution of 39.6μm; Siemens Inveon scanner), which included respiratory and cardiac gating, nine weeks after placement of the cuff to reconstruct the *in vivo* geometry of both the diseased and control arteries. Pulsed Doppler ultrasound measurements (Vevo 770 Visualsonics) of blood velocity at the inlet of each carotid artery were conducted 1–3 days after micro-CT imaging. The

mouse was then euthanized, its vessels perfusion-fixed, both carotid arteries were dissected, snap-frozen in OCT and stored for histological processing. Tissue blocks were serially sectioned from the aortic arch to the carotid bifurcation, stained using oil red O (ORO) to identify plaque structure and lipid concentration, and imaged at 10x magnification.

Three-dimensional (3D) reconstructions of the lumen of the control and instrumented vessels were obtained from the back-projected micro-CT slices using a level-set segmentation method. Reconstruction of the vessel wall was obtained through a multistep process that involved co-registration of histology to the reconstructed vessel lumen (Segers et al., 2007). Briefly, the imaged histological sections were manually segmented (to identify the lumen, internal elastic lamina, and external elastic lamina), binarized using a threshold to identify lipid staining, and digitized in Clemex. These data were then imported into a custom MATLAB program that performed co-registration using the aortic arch, cuff region, and carotid bifurcation of the lumen as landmarks, which corrected for longitudinal shrinkage. Circumferential co-registration was done by placing an ink line on the outer curvature of the artery prior to isolation. Radial co-registration of histology was performed by warping the histology on the 3D reconstructed vessel lumen assuming isotropic shrinkage of the vessel wall. Wall thickness and lipid stain information from histology was then interpolated over the nodes of the reconstructed lumen. The control vessel was also reconstructed from micro-CT, but only simulated using a nominal thickness.

The meshing of the vessel lumen uses the lumen wall outline STL reconstructed from micro-CT. The mesh was created with linear hexahedral elements with a boundary layer mesh of 10% of the radius consisting of three layers with growth rate of 1.2. The vessel wall was meshed using a custom program in MATLAB, which also employed hexahedral elements. The nodes on the luminal surface were located to coincide with the nodes on the inner wall of the artery mesh to improve the FSI interaction efficiency. Convergence tests were performed to identify a final mesh density that demonstrated less than 1% error for both stress/strain in the wall and shear stress in the lumen.

2.2 Material Properties

Mechanical properties for the artery wall were obtained from previously reported mechanical behaviour data from inflation testing of wild type mouse carotid arteries (Eberth et al., 2009) . These data demonstrated a nonlinear elastic mechanical behaviour over finite strains that was modelled using the isotropic Ogden hyper-elastic constitutive relation. The Ogden strain energy function, *W*, is given by

$$W = \sum_{i=1}^{N} \frac{2\mu_i}{\alpha_i^2}\left(\lambda_1^{\alpha_i} + \lambda_2^{\alpha_i} + \lambda_3^{\alpha_i} - 3\right), \quad (1)$$

where μ, α, and N are material parameters and λ_i are the principal stretches in the circumferential, axial, and radial directions. These material parameters were identified for the non-diseased portions of the artery wall through a nonlinear regression to previously reported inflation data (Cauchy stress versus stretch) for the wild type mouse carotid artery (Eberth et al., 2009); best-fit parameters were: μ_1=20.56, α_1=1e-5, μ_2=0.785, α_2=10.10, which demonstrated an excellent fit to the data (**Fig. 1A**). In plaque regions with lipid uptake, the same Ogden model was used and the μ_i parameters were scaled based on the ratio of previously reported stiffness values of lipid-rich areas of plaque to normal wall (**Fig. 1B**) (Tracqui et al., 2011). Lipid stain intensities from the digitized and co-registered histology were separated into two different diseased material types based on the degree of staining. The stiffness of each material, assessed for each element of the model, was reduced to 50% and 30% of normal (i.e., no staining), respectively, based on the degree of lipid staining. The normal and diseased components of the vessel wall were given a density of 1050 kg/m^3 and Poisson's ratio of 0.495 (nearly incompressible, which is appropriate because the artery wall is 70% to 80% water by weight and exhibits nearly isochoric motions under physiologic loads (Humphrey, 2002)).

To account for the stability afforded by the carotid sheath that surrounds the carotid artery *in vivo*, perivascular tissue was modelled by adding a linear elastic material layer around and attached to the outermost vessel layer with an elastic modulus of 28 Pa and Poisson's ratio of 0.05 (highly

compressible). The thickness and material properties were optimized to minimize the impact on the vessel wall's dilatation at 80 mmHg and 120 mmHg pressurisation.

Blood was modelled as an incompressible non-Newtonian fluid using the Carreau-Yasuda model, (Johnston et al., 2004) given by

$$\eta = \eta_\infty + (\eta_0 - \eta_\infty)(1 + (\lambda\dot{\gamma})^\alpha)^{\frac{n-1}{\alpha}}, \quad (2)$$

where parameters were chosen to be η_∞= 55 Pa.s, η_0 = 3.45 Pa.s, λ=3.313, n=0.3568, α=2. Blood density was also prescribed as 1050 kg/m^3.

2.3 Finite element modelling of artery pre-stresses

Multiple studies (Debes and Fung, 1995; Guo et al., 2005; Matsumoto and Hayashi, 1996; Otoguro et al., 2015; Taber, 2001) indicate that the *in vivo* arterial wall in diastole is exposed to a circumferential residual stress (i.e., stress that exists in the absence of applied loads) and an axial prestress due to elongation in situ (Cardamone et al., 2009; Guo et al., 2005; Maes et al., 2019; Taber, 2001). In addition, the *in vivo* artery is prestressed by end-diastolic blood pressure. To account for this initial stress state, sequential solids-only simulations were run in Abaqus (v6.14), where the final stress field from each simulation was used as the initial condition for the next simulation, as follows. First, circumferential residual stress was determined by using a straightened-equivalent artery model with a circumferential opening of 92^o (Hansen et al., 2013) that was closed through application of a rotation to connect one side of the opening to the other, which was held fixed. Second, axial prestress was determined by applying a 40 kPa axial load (Gleason et al., 2007). The load was applied over 10 steps using the Backward Incremental method (de Putter et al., 2007; Speelman et al., 2009), which utilises the *in vivo* geometry from micro-CT as the initial geometry for each simulation, with the computed resultant stress field from the prior step providing the model stress for initialisation of the subsequent step. Third, the blood pressure prestress was obtained by applying 80 mmHg over 12 steps, again using the Backward Incremental method. All simulations in the pressurisation steps were constrained axially

at both ends. The computed stress field from the final simulation (referred to simply as “prestresses” or the prestressed configuration) was used as the initial stress state of the FSI model.

2.4 FSI modelling

The FSI simulations were performed with Abaqus/Standard 6.14 and Abaqus/CFD 6.14 modules (Dassault Systems) as part of a co-simulation based on the Arbitrary Lagrangian-Eulerian (ALE) method. In this approach, the mesh is conserved between the fluid-solid interface at the inner surface of the vessel wall, the pressure and the shear stresses are passed from the blood flow side of this interface to the vessel wall, and the wall displacement and actual diameters are passed from the vessel side to the fluid domain simulation.

For the control vessel FSI model, the nominal vessel thickness was assumed to be a constant value of 50 μm and the prestresses for this model were computed using the vessel geometry with the aforementioned nominal thickness. For the instrumented or cuffed vessel, three FSI models were formulated as follows:

A) Nominal Model	Nominal thickness and homogenous wall material FSI model with the prestresses.
B) Histology Model	Histology-based wall thickness FSI model with heterogeneous wall material properties based on the degree of lipid staining initialised before computing the prestresses.
C) Hybrid Model	Histology-based wall thickness FSI model with heterogeneous wall material properties and prestresses obtained from the Histology Model (B), but with homogeneous material properties. This aims to represent the prestresses that largely develop during normal (healthy) vessel wall growth, prior to the development of atherosclerosis due to cuff placement. In this model, prestresses calculated in the regions of lipid deposition were set to zero.

2.4.1 Boundary conditions

A blood velocity waveform was measured by Doppler ultrasound (Vevo 770) for each carotid artery and applied to the inlet of each model with a prescribed parabolic profile. An outlet boundary model (Pahlevan et al., 2011) was added to simulate the compliance and resistance of the downstream vasculature. The compliance of 2.5E-14 m^4s^2/kg was computed using previously published values for compliance and resistance (Aslanidou et al., 2016). Resistance was optimised to achieve 80 mmHg diastolic pressure. All additional boundary conditions are given in **Table S1** (**Appendix A)**.

2.5 Shear and strain metrics

The TAWSS was calculated for each element on the lumen wall over one cardiac cycle (Pedrigi et al., 2016). In addition, endothelial strain was reported based on logarithmic strain obtained from the FSI models for the innermost elements of the artery. The strain field in the FSI model stems from a combination of strains developed from the prestresses and the pulsatile pressure over the cardiac cycle (**Fig. 2**). Since endothelial cells have a short half-life (20 – 40 days), their stress-free length is reasonably assumed to be at diastole. In addition, endothelial cell function is likely most impacted by the circumferential strain of the artery because this direction experiences the largest change in strain over the cardiac cycle (Pedrigi et al., 2017). Thus, herein, we focused on cyclic circumferential strain, computed as the difference between systole and diastole.

3. Results

The control vessel FSI simulations produced pressures of 82/110 mmHg and a peak physiologic dilatation of 11.6% (**Fig. 3**). Time-averaged wall shear stress maps for all models are given in **Fig. S2** (**Appendix A)**.

3.1. A novel Hybrid FSI Model predicts altered strain in local regions of plaque

An important aim in this study was to develop FSI models with all relevant prestresses which captured local heterogeneities in the strain field that resulted from altered plaque properties. We began with the Histology Model of the instrumented artery (for definition see above), where softer material properties in regions of lipid deposition were initialized *before* computing prestresses. This model predicted a median circumferential strain in the plaque regions of 5.8% (**Fig. 4C**). Interestingly, this was slightly *less* than the 6.1% within the same spatial locations of the Nominal Model, which does not consider softer properties due to lipid deposition. Since the FSI model should predict higher strains in local regions of the atherosclerotic artery that are more compliant due to the presence of lipids, we developed a hybrid approach where prestresses were computed using normal material properties over the whole artery and set to zero in regions of lipid deposition. The Hybrid Model exhibited the expected increased compliance in the plaque regions compared to the other models with a median circumferential strain of 7.0% (**Fig. 4C**). A similar trend was observed with the radial strain, whereby the Hybrid Model exhibited the largest (compressive) radial strain in regions of lipid deposition of -7.0% compared to -5.2% and -5.7% in the Histology Model and Nominal Model, respectively (**Fig. S3**). Strain in the axial direction showed little change over the cardiac cycle (**Fig. S4**, **Appendix A**).

To further demonstrate the robustness of the Hybrid Model, we also evaluated whether it could predict realistic changes in artery wall strain with *increased* stiffness of the plaque regions, such as occurs with a fibrous cap atheroma. This Hybrid-Stiff Model was simulated with an arbitrary 10-fold increase in stiffness of the lipid regions. It predicted the expected lower circumferential strain within these regions of 4.6% compared to both the softer properties of the Hybrid Model and normal properties of the Nominal model (**Fig. 5**). These results demonstrate that our hybrid approach is capable of capturing changes in local stiffness in diseased arteries.

To better understand the resultant circumferential strains exhibited by the different FSI models, we also evaluated diameter over the length of the instrumented artery in the prestressed configuration (before starting the FSI simulation), diastole, and systole. As expected, we found that,

the diameter of the artery after computing the prestresses in the Nominal Model and Histology Model was nearly identical to that in the FSI simulations during diastole, which results from using the Backward Incremental method to compute prestresses. In contrast, it was significantly larger in the hybrid models in regions of lipid deposition, where prestresses were set to zero, at both diastole and systole (**Fig. 6**). As a result, circumferential strain at systole computed relative to the prestressed configuration was 30.5% in the Hybrid Model and 11.8% in the Hybrid-Stiff Model, compared to 7.1% and 7.7% in the Histology Model and Nominal Model, respectively.

3.2. The Hybrid Model predicts lower TAWSS than the other FSI models and CFD

The Nominal Model with uniform material properties predicted a median difference in TAWSS compared to the corresponding CFD simulation over the whole vessel (outside of the cuff) of -11.5% (**Fig. 7A-B**). To our surprise, the Histology Model predicted a TAWSS profile over the whole vessel that was nearly identical to the Nominal Model with a median difference in TAWSS compared to CFD of -11.2%. Correspondingly, the median difference in TAWSS between each of these FSI models and CFD within only the plaque regions was similar for the Histology Model compared to the Nominal Model with values of -11.3% and -12.0%, respectively (**Fig. 7C**). In contrast, the Hybrid Model resulted in a much larger median difference in TAWSS from CFD in the plaque regions of -23.8%, but was similar over the artery as a whole with a difference of -11.4% (**Fig. 7A-C**). These results demonstrate that predictions of endothelial shear stress are not only lower in an FSI model, in general, but, in the case of the Hybrid Model, are also more heterogeneous due to the effect of altered properties in regions of plaque.

4. Discussion

This paper presents the development of FSI models of an atherosclerotic with local tissue properties and normal carotid artery from an $ApoE^{-/-}$ mouse. We found that the normal artery model predicted physiologically accurate values for blood pressure, vessel dilatation, and flow, comparable

to previously reported measurements in mice (De Wilde et al., 2016a; De Wilde et al., 2016b). To our knowledge, only one other group has developed an FSI model of the mouse carotid artery (De Wilde et al., 2016a; De Wilde et al., 2016b; De Wilde et al., 2016c), but this work had a lesser emphasis on the endothelial wall mechanics, including no consideration of altered wall properties with plaque development. The focus of our paper was the development of an FSI model with altered properties in regions of lipid deposition to evaluate how different modelling assumptions related to the incorporation of "prestresses" within the artery wall (i.e., circumferential residual stress and prestresses due to axial elongation and diastolic blood pressure) affect prediction of endothelial shear stress and strain. Since murine atherosclerosis is often associated with lipid-rich plaques, probably due to the extremely high cholesterol levels that are achieved through genetic modification and diet to accelerate atherosclerosis (Tang et al., 2005; Tracqui et al., 2011), we focused plaque properties solely on the presence of softer lipids within local regions of the Histology Model and hybrid models, which were assigned based on co-registered, serially-collected oil red O-stained histology sections (an approach called 3-D histology) (Segers et al., 2007).

We found that incorporating these local changes in wall properties *prior* to the calculation of prestresses via the Histology Model led to almost no difference in either circumferential strain or TAWSS as compared to the Nominal Model with normal properties, even in plaque regions. This was due to the formation of higher strains within the more compliant regions of lipid deposition in the Histology Model that caused a stiffening effect from the nonlinear material properties. As a result, the lipid regions at the start of the FSI simulation had similar stress and stiffness to the surrounding normal wall (**Fig. S5**, **Appendix A**). To avoid this problem, the Hybrid Model calculated the prestresses using normal wall properties over the entire vessel (even in plaque regions) and only incorporated them into the non-diseased regions, with regions of lipid deposition assumed to be stress-free at the start of the FSI simulation. This model predicted the expected increased compliance and decreased TAWSS on the endothelium overlaying the plaques. Thus, we found that plaque properties should be introduced into an FSI model after the calculation of prestresses. This is significant because it aligns

with other studies that have shown residual stress and prestresses to depend primarily on elastin, not collagen, which is deposited during normal (healthy) vessel wall growth and has a half-life comparable to the lifespan of the organism (Cardamone et al., 2009), so exists prior to the development of atherosclerosis.

4.1. Limitations

There are three primary limitations to consider in this study. First, we performed FSI modelling on the atherosclerotic and non-atherosclerotic carotid arteries from only one mouse. Since the purpose of this study was to describe the development of the FSI models and evaluate how different assumptions related to the incorporation of prestresses affect prediction of endothelial shear stress and strain, not to demonstrate connections between mechanical metrics and the associated pathobiology, one mouse is sufficient because these assumptions are independent of the specific arteries used (i.e., geometries, mechanical properties and blood velocities). Second, a common limitation of murine arterial wall modelling is the lack of local temporal pressure measurements. Pressure measurements are difficult to obtain in mice due to their small size. Tail pressure measurements are available, but these are not sufficiently accurate or acquired in the area of interest, so are not considered suitable replacements for carotid artery pressure (Zhao et al., 2011). Other invasive methods require sacrificing the animal. We opted for a boundary model based on both measured and estimated compliance and resistance values for downstream mouse vasculature. This outlet model results in a vessel distension that compares well with M-mode measurements (**Fig. 3B**). Third, mechanical properties used for the artery wall were based on a fit of the isotropic Ogden model to previously reported experimental inflation data from wild-type mice (Eberth et al., 2009). We justified the use of an isotropic model based on the small degree of anisotropy between the mean axial and circumferential mechanical behaviour curves obtained from the defined constitutive model for several mice in this previous study.

4.2. Conclusions

This study describes the influence of assumptions in the development of FSI models of locally diseased blood vessels on the prediction of endothelial shear stress and strain. We found that prestresses should be computed using normal material properties and assigned only to non-diseased regions of the artery wall; plaque regions should have zero stress at the start of the FSI simulation. Using this approach, we also found that FSI predicted significantly lower endothelial shear stress compared to CFD and that this difference was even greater in regions of lipid deposition. This resulted in significant heterogeneity of endothelial shear stress in the atherosclerotic artery due to variations in stiffness and, in turn, wall strain. Since such variations cannot be captured by CFD, this finding demonstrates that FSI more accurately predicts shear stress in atherosclerotic arteries, which may increase predictability of associated biomarkers of plaque development. Further studies are needed with a larger cohort of mice to address improved prediction of plaque development using FSI compared to CFD.

Figure Legends

Fig. 1. Mechanical behaviour of the normal and atherosclerotic carotid artery models. (A) Comparison of the mechanical behaviour from empirical inflation data (Eberth et al., 2009), the fit of the Ogden hyperelastic model, and simulated equibiaxial testing using FEA. (B) The Ogden model used for the normal artery wall (solid line) and regions of lipid deposition (dashed lines), wherein the stiffness of the latter was reduced to 50% and 30% of the normal stiffness, respectively, based on the degree of lipid staining.

Fig. 2. Illustration of the nonlinear mechanical behaviour of the mouse carotid artery from the stress-free configuration. Diagram shows the strain due to the different prestresses and then additional strain induced by the cardiac cycle, called cyclic strain.

Fig. 3. Comparison of simulation model boundary conditions and radial displacement versus *in vivo* measurements from ultrasound. (A) Inlet flow velocity closely matched the flow velocity prescribed at the start of the inlet extension with the pressure waveform generated via the outlet boundary model. (B) FSI artery dilatation (% change in radius) compares well to empirical measurements from ultrasound.

Fig. 4. Cyclic circumferential logarithmic strain (%) from FSI simulations of the Nominal Model, Histology Model, and Hybrid Model. (A) 2D projections of each metric from the 3D artery from near the aortic arch (top) to just before the carotid bifurcation (bottom) showing the distribution of oil red O (lipid) staining and circumferential logarithmic strain (%) at the inner lining of the artery (endothelial strain) from the FSI simulations. (B-C) Histograms of the number of elements (count) for each increment of circumferential logarithmic strain (0.3%) in FSI (B) over the whole artery (excluding the cuff area) and (C) only in regions of lipid deposition (plaque) for each of the three models.

Fig. 5. Cyclic circumferential logarithmic strain (%) from FSI simulations of the Histology Model, Hybrid Model, and Hybrid-Stiff Model. (A) 2D projections of each metric from the 3D artery from near the aortic arch (top) to just before the carotid bifurcation (bottom) showing the distribution of oil red O (lipid) staining and circumferential logarithmic strain (%) at the inner lining of the artery (endothelial strain) from the FSI simulations. (B-C) Histograms of the number of elements (count) for each increment of circumferential logarithmic strain (0.3%) in FSI (B) over the whole artery (excluding the cuff area) and (C) only in regions of lipid deposition (plaque) for each of the three models.

Fig. 6. Diameter of the instrumented carotid artery from the inlet (near the aortic arch) to the outlet (near the carotid bifurcation) for the (A) Nominal Model, (B) Histology Model, (C) Hybrid Model, and (D) Hybrid-Stiff Model. Region of cuff placement is lightly greyed. *Indicates the center of the upstream plaque, where the Hybrid Model exhibited increased dilatation compared to the other models due to the softer lipid properties and method of incorporating the prestresses. Because this method involved setting the final prestress in the lipid regions to zero, this increased dilatation of the Hybrid Model was seen both at diastole (compared to the prestressed configuration) and over the cardiac cycle.

Fig. 7. The percent difference in TAWSS (ΔTAWSS) of FSI relative to CFD simulations for the Nominal Model, Histology Model, and Hybrid Model. (A) 2D projections of each metric on the artery from near the aortic arch (top) to just before the carotid bifurcation (bottom) showing the distribution of oil red O (lipid) staining and ΔTAWSS of FSI relative to the same model in CFD. (B-C) Histograms of the number of elements (count) for each increment of ΔTAWSS (1%) in FSI (B) over the whole artery (excluding the cuff area) and (C) only in regions of lipid deposition (plaque) for each of the three models.

Conflict of interest statement

None.

Acknowledgments

We gratefully acknowledge financial support for this work from the British Heart Foundation grants RG/11/12/29055 and PG/15/49/31595, US National Institute of Biomedical Imaging and Bioengineering of the National Institutes of Health grant R03EB026837, and US National Science Foundation CAREER award CMMI-1944131. Also, thanks to Clint Davies at SIMULIA with Abaqus.

References

Alberts-Grill, N., Denning, T.L., Rezvan, A., Jo, H., 2013. The role of the vascular dendritic cell network in atherosclerosis. Am J Physiol Cell Physiol 305, C1-21. https://doi.org/10.1152/ajpcell.00017.2013

Aslanidou, L., Trachet, B., Reymond, P., Fraga-Silva, R.A., Segers, P., Stergiopulos, N., 2016. A 1D model of the arterial circulation in mice. ALTEX 33, 13-28. https://doi.org/10.14573/altex.1507071

Cardamone, L., Valentin, A., Eberth, J.F., Humphrey, J.D., 2009. Origin of axial prestretch and residual stress in arteries. Biomech Model Mechanobiol 8, 431-446. https://doi.org/10.1007/s10237-008-0146-x

Cheng, C., Tempel, D., van Haperen, R., van der Baan, A., Grosveld, F., Daemen, M.J., Krams, R., de Crom, R., 2006. Atherosclerotic lesion size and vulnerability are determined by patterns of fluid shear stress. Circulation 113, 2744-2753. https://doi.org/10.1161/CIRCULATIONAHA.105.590018

Chester, A.H., El-Hamamsy, I., Butcher, J.T., Latif, N., Bertazzo, S., Yacoub, M.H., 2014. The living aortic valve: From molecules to function. Glob Cardiol Sci Pract 2014, 52-77. https://doi.org/10.5339/gcsp.2014.11

Chistiakov, D.A., Revin, V.V., Sobenin, I.A., Orekhov, A.N., Bobryshev, Y.V., 2015. Vascular Endothelium: Functioning in Norm, Changes in Atherosclerosis and Current Dietary Approaches to improve Endothelial Function. Mini reviews in medicinal chemistry.

de Putter, S., Wolters, B.J., Rutten, M.C., Breeuwer, M., Gerritsen, F.A., van de Vosse, F.N., 2007. Patient-specific initial wall stress in abdominal aortic aneurysms with a backward incremental method. J Biomech 40, 1081-1090. https://doi.org/10.1016/j.jbiomech.2006.04.019

De Wilde, D., Trachet, B., De Meyer, G., Segers, P., 2016a. The influence of anesthesia and fluid-structure interaction on simulated shear stress patterns in the carotid bifurcation of mice. J Biomech 49, 2741-2747. https://doi.org/10.1016/j.jbiomech.2016.06.010

De Wilde, D., Trachet, B., De Meyer, G.R.Y., Segers, P., 2016b. Shear Stress Metrics and Their Relation to Atherosclerosis: An In Vivo Follow-up Study in Atherosclerotic Mice. Ann Biomed Eng 44, 2327-2338. https://doi.org/10.1007/s10439-015-1540-z

De Wilde, D., Trachet, B., Debusschere, N., Iannaccone, F., Swillens, A., Degroote, J., Vierendeels, J., De Meyer, G.R.Y., Segers, P., 2016c. Assessment of shear stress related parameters in the carotid bifurcation using mouse-specific FSI simulations. J Biomech 49, 2135-2142. https://doi.org/10.1016/j.jbiomech.2015.11.048

Debes, J.C., Fung, Y.C., 1995. Biaxial mechanics of excised canine pulmonary arteries. Am J Physiol 269, H433-442. https://doi.org/10.1152/ajpheart.1995.269.2.H433

Eberth, J.F., Taucer, A.I., Wilson, E., Humphrey, J.D., 2009. Mechanics of carotid arteries in a mouse model of Marfan Syndrome. Ann Biomed Eng 37, 1093-1104. https://doi.org/10.1007/s10439-009-9686-1

Fung, Y.C., 1991. What are the residual stresses doing in our blood vessels? Ann Biomed Eng 19, 237-249.

Gleason, R.L., Wilson, E., Humphrey, J.D., 2007. Biaxial biomechanical adaptations of mouse carotid arteries cultured at altered axial extension. J Biomech 40, 766-776. https://doi.org/10.1016/j.jbiomech.2006.03.018

Guo, X., Lu, X., Kassab, G.S., 2005. Transmural strain distribution in the blood vessel wall. Am J Physiol Heart Circ Physiol 288, H881-886. https://doi.org/10.1152/ajpheart.00607.2004

Hansen, L., Parker, I., Sutliff, R.L., Platt, M.O., Gleason, R.L., Jr., 2013. Endothelial dysfunction, arterial stiffening, and intima-media thickening in large arteries from HIV-1 transgenic mice. Ann Biomed Eng 41, 682-693. https://doi.org/10.1007/s10439-012-0702-5

Humphrey, J.D., 2002. Cardiovascular Solid Mechanics: Cells, Tissues, and Organs. Springer-Verlag, New York.
Johnston, B.M., Johnston, P.R., Corney, S., Kilpatrick, D., 2004. Non-Newtonian blood flow in human right coronary arteries: steady state simulations. J Biomech 37, 709-720. https://doi.org/10.1016/j.jbiomech.2003.09.016
Kobielarz, M., Kozun, M., Gasior-Glogowska, M., Chwilkowska, A., 2020. Mechanical and structural properties of different types of human aortic atherosclerotic plaques. J Mech Behav Biomed Mater 109, 103837. https://doi.org/10.1016/j.jmbbm.2020.103837
Krams, R., Verheye, S., van Damme, L.C., Tempel, D., Mousavi Gourabi, B., Boersma, E., Kockx, M.M., Knaapen, M.W., Strijder, C., van Langenhove, G., Pasterkamp, G., van der Steen, A.F., Serruys, P.W., 2005. In vivo temperature heterogeneity is associated with plaque regions of increased MMP-9 activity. Eur Heart J 26, 2200-2205. https://doi.org/10.1093/eurheartj/ehi461
Kwak, B.R., Back, M., Bochaton-Piallat, M.L., Caligiuri, G., Daemen, M.J., Davies, P.F., Hoefer, I.E., Holvoet, P., Jo, H., Krams, R., Lehoux, S., Monaco, C., Steffens, S., Virmani, R., Weber, C., Wentzel, J.J., Evans, P.C., 2014. Biomechanical factors in atherosclerosis: mechanisms and clinical implications. Eur Heart J 35, 3013-3020, 3020a-3020d. https://doi.org/10.1093/eurheartj/ehu353
Liu, X.M., Peyton, K.J., Durante, W., 2013. Physiological cyclic strain promotes endothelial cell survival via the induction of heme oxygenase-1. Am J Physiol Heart Circ Physiol 304, H1634-1643. https://doi.org/10.1152/ajpheart.00872.2012
Maes, L., Fehervary, H., Vastmans, J., Mousavi, S.J., Avril, S., Famaey, N., 2019. Constrained mixture modeling affects material parameter identification from planar biaxial tests. J Mech Behav Biomed Mater 95, 124-135. https://doi.org/10.1016/j.jmbbm.2019.03.029
Matsumoto, T., Hayashi, K., 1996. Stress and strain distribution in hypertensive and normotensive rat aorta considering residual strain. J Biomech Eng 118, 62-73. https://doi.org/10.1115/1.2795947
Morbiducci, U., Kok, A.M., Kwak, B.R., Stone, P.H., Steinman, D.A., Wentzel, J.J., 2016. Atherosclerosis at arterial bifurcations: evidence for the role of haemodynamics and geometry. Thromb Haemost 115, 484-492. https://doi.org/10.1160/TH15-07-0597
Otoguro, S., Hayashi, Y., Miura, T., Uehara, N., Utsumi, S., Onuki, Y., Obata, Y., Takayama, K., 2015. Numerical Investigation of the Residual Stress Distribution of Flat-Faced and Convexly Curved Tablets Using the Finite Element Method. Chem Pharm Bull (Tokyo) 63, 890-900. https://doi.org/10.1248/cpb.c15-00481
Pahlevan, N.M., Amlani, F., Hossein Gorji, M., Hussain, F., Gharib, M., 2011. A physiologically relevant, simple outflow boundary model for truncated vasculature. Ann Biomed Eng 39, 1470-1481. https://doi.org/10.1007/s10439-011-0246-0
Pedrigi, R.M., de Silva, R., Bovens, S.M., Mehta, V.V., Petretto, E., Krams, R., 2014. Thin-cap fibroatheroma rupture is associated with a fine interplay of shear and wall stress. Arterioscler Thromb Vasc Biol 34, 2224-2231. https://doi.org/10.1161/ATVBAHA.114.303426
Pedrigi, R.M., Mehta, V.V., Bovens, S.M., Mohri, Z., Poulsen, C.B., Gsell, W., Tremoleda, J.L., Towhidi, L., de Silva, R., Petretto, E., Krams, R., 2016. Influence of shear stress magnitude and direction on atherosclerotic plaque composition. R Soc Open Sci 3, 160588. https://doi.org/10.1098/rsos.160588
Pedrigi, R.M., Papadimitriou, K.I., Kondiboyina, A., Sidhu, S., Chau, J., Patel, M.B., Baeriswyl, D.C., Drakakis, E.M., Krams, R., 2017. Disturbed Cyclical Stretch of Endothelial Cells Promotes Nuclear Expression of the Pro-Atherogenic Transcription Factor NF-kappaB. Ann Biomed Eng 45, 898-909. https://doi.org/10.1007/s10439-016-1750-z
Pedrigi, R.M., Poulsen, C.B., Mehta, V.V., Ramsing Holm, N., Pareek, N., Post, A.L., Kilic, I.D., Banya, W.A., Dall'Ara, G., Mattesini, A., Bjorklund, M.M., Andersen, N.P., Grondal, A.K., Petretto, E., Foin, N., Davies, J.E., Di Mario, C., Fog Bentzon, J., Erik Botker, H., Falk, E., Krams, R., de Silva,

R., 2015. Inducing Persistent Flow Disturbances Accelerates Atherogenesis and Promotes Thin Cap Fibroatheroma Development in D374Y-PCSK9 Hypercholesterolemic Minipigs. Circulation 132, 1003-1012. https://doi.org/10.1161/CIRCULATIONAHA.115.016270

Peters, A.S., Brunner, G., Krieg, T., Eckes, B., 2015. Cyclic mechanical strain induces TGFbeta1-signalling in dermal fibroblasts embedded in a 3D collagen lattice. Arch Dermatol Res 307, 191-197. https://doi.org/10.1007/s00403-014-1514-2

Segers, D., Helderman, F., Cheng, C., van Damme, L.C., Tempel, D., Boersma, E., Serruys, P.W., de Crom, R., van der Steen, A.F., Holvoet, P., Krams, R., 2007. Gelatinolytic activity in atherosclerotic plaques is highly localized and is associated with both macrophages and smooth muscle cells in vivo. Circulation 115, 609-616. https://doi.org/10.1161/CIRCULATIONAHA.106.636415

Speelman, L., Bosboom, E.M., Schurink, G.W., Buth, J., Breeuwer, M., Jacobs, M.J., van de Vosse, F.N., 2009. Initial stress and nonlinear material behavior in patient-specific AAA wall stress analysis. J Biomech 42, 1713-1719. https://doi.org/10.1016/j.jbiomech.2009.04.020

Stone, P.H., Maehara, A., Coskun, A.U., Maynard, C.C., Zaromytidou, M., Siasos, G., Andreou, I., Fotiadis, D., Stefanou, K., Papafaklis, M., Michalis, L., Lansky, A.J., Mintz, G.S., Serruys, P.W., Feldman, C.L., Stone, G.W., 2018. Role of Low Endothelial Shear Stress and Plaque Characteristics in the Prediction of Nonculprit Major Adverse Cardiac Events: The PROSPECT Study. JACC Cardiovasc Imaging 11, 462-471. https://doi.org/10.1016/j.jcmg.2017.01.031

Taber, L.A., 1995. Biomechanics of Growth, Remodeling, and Morphogenesis. Applied Mechanics Reviews 48, 487-545. https://doi.org/10.1115/1.3005109

Taber, L.A., 2001. Stress-Modulated Growth, Residual Stress, and Vascular Heterogeneity. Journal of Biomechanical Engineering 123, 528-535.

Tang, D., Yang, C., Zheng, J., Woodard, P.K., Saffitz, J.E., Sicard, G.A., Pilgram, T.K., Yuan, C., 2005. Quantifying effects of plaque structure and material properties on stress distributions in human atherosclerotic plaques using 3D FSI models. J Biomech Eng 127, 1185-1194. https://doi.org/10.1115/1.2073668

Tian, J., Ren, X., Uemura, S., Dauerman, H., Prasad, A., Toma, C., Jia, H., Abtahian, F., Vergallo, R., Hu, S., McNulty, I., Lee, H., Lee, S., Yu, B., Jang, I.K., 2014. Spatial heterogeneity of neoatherosclerosis and its relationship with neovascularization and adjacent plaque characteristics: optical coherence tomography study. Am Heart J 167, 884-892 e882. https://doi.org/10.1016/j.ahj.2014.03.013

Trachet, B., Bols, J., Degroote, J., Verhegghe, B., Stergiopulos, N., Vierendeels, J., Segers, P., 2015. An animal-specific FSI model of the abdominal aorta in anesthetized mice. Ann Biomed Eng 43, 1298-1309. https://doi.org/10.1007/s10439-015-1310-y

Tracqui, P., Broisat, A., Toczek, J., Mesnier, N., Ohayon, J., Riou, L., 2011. Mapping elasticity moduli of atherosclerotic plaque in situ via atomic force microscopy. J Struct Biol 174, 115-123. https://doi.org/10.1016/j.jsb.2011.01.010

Trogan, E., Choudhury, R.P., Dansky, H.M., Rong, J.X., Breslow, J.L., Fisher, E.A., 2002. Laser capture microdissection analysis of gene expression in macrophages from atherosclerotic lesions of apolipoprotein E-deficient mice. Proc Natl Acad Sci U S A 99, 2234-2239. https://doi.org/10.1073/pnas.042683999

Yurdagul, A., Jr., Finney, A.C., Woolard, M.D., Orr, A.W., 2016. The arterial microenvironment: the where and why of atherosclerosis. Biochem J 473, 1281-1295. https://doi.org/10.1042/BJ20150844

Zhao, X., Ho, D., Gao, S., Hong, C., Vatner, D.E., Vatner, S.F., 2011. Arterial Pressure Monitoring in Mice. Curr Protoc Mouse Biol 1, 105-122. https://doi.org/10.1002/9780470942390.mo100149

Figure

Click here to access/download;Figure;Fig1.tif

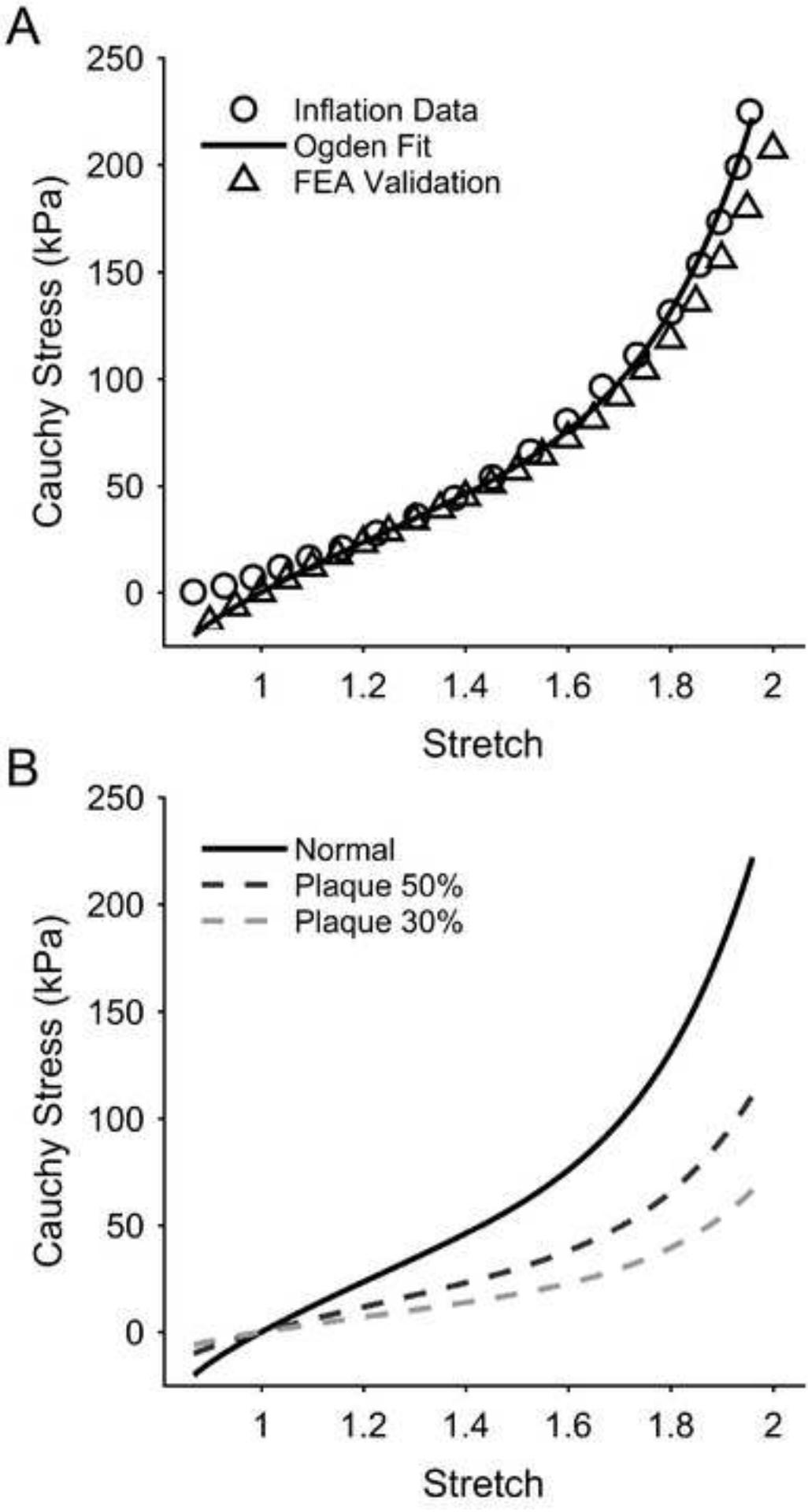

Figure

Click here to access/download;Figure;Fig2.tif

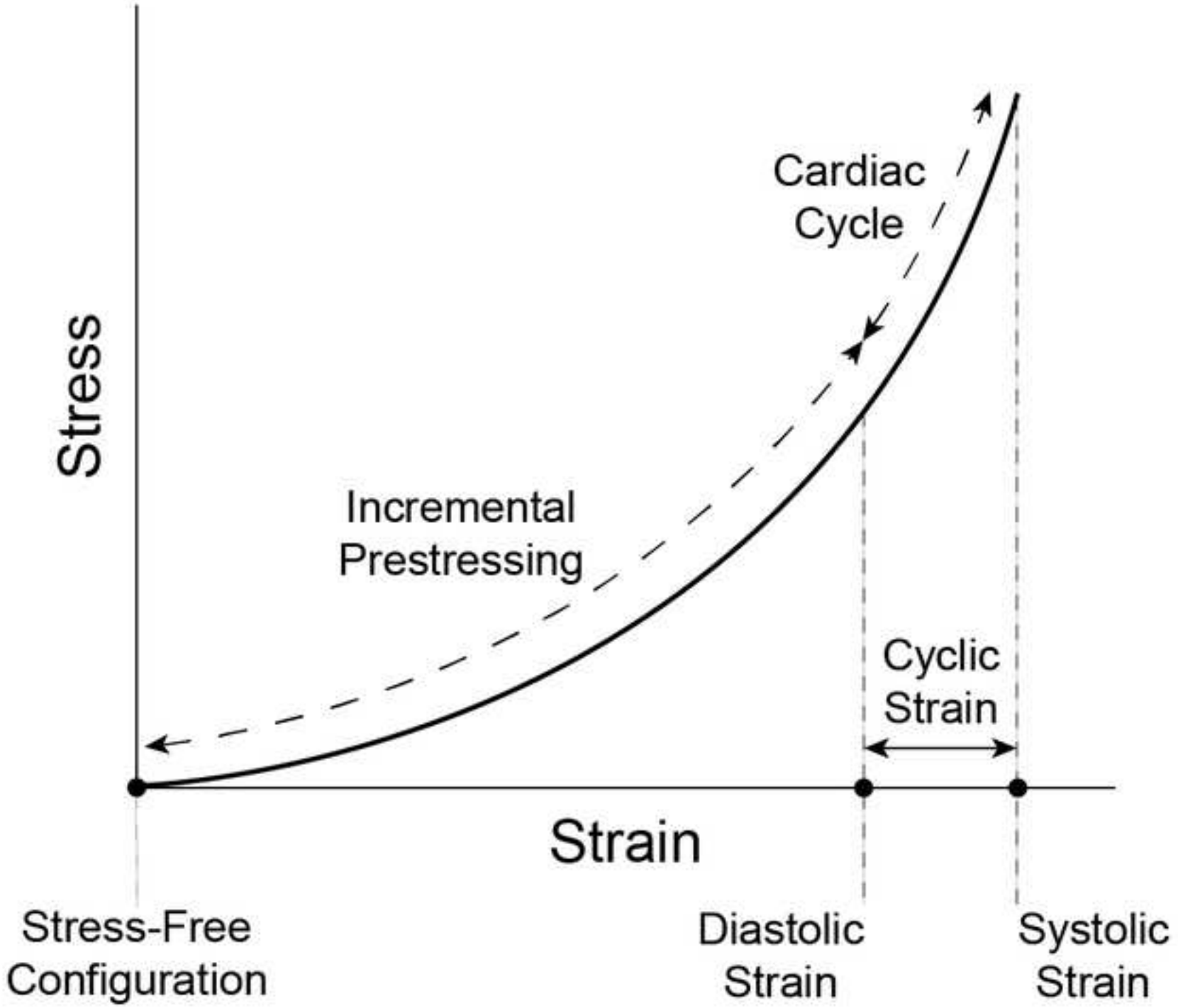

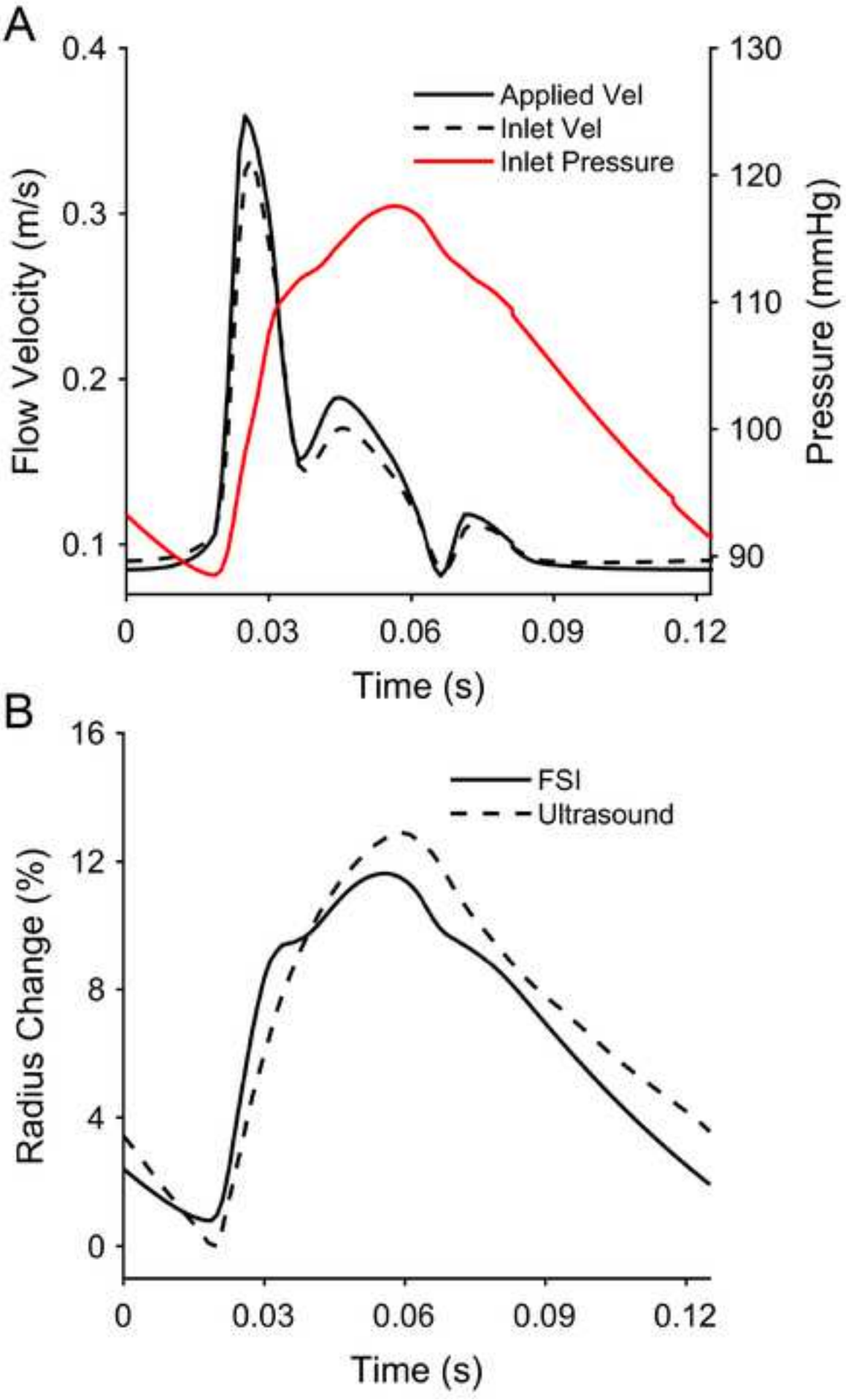

Figure

Click here to access/download;Figure;Fig4.tif

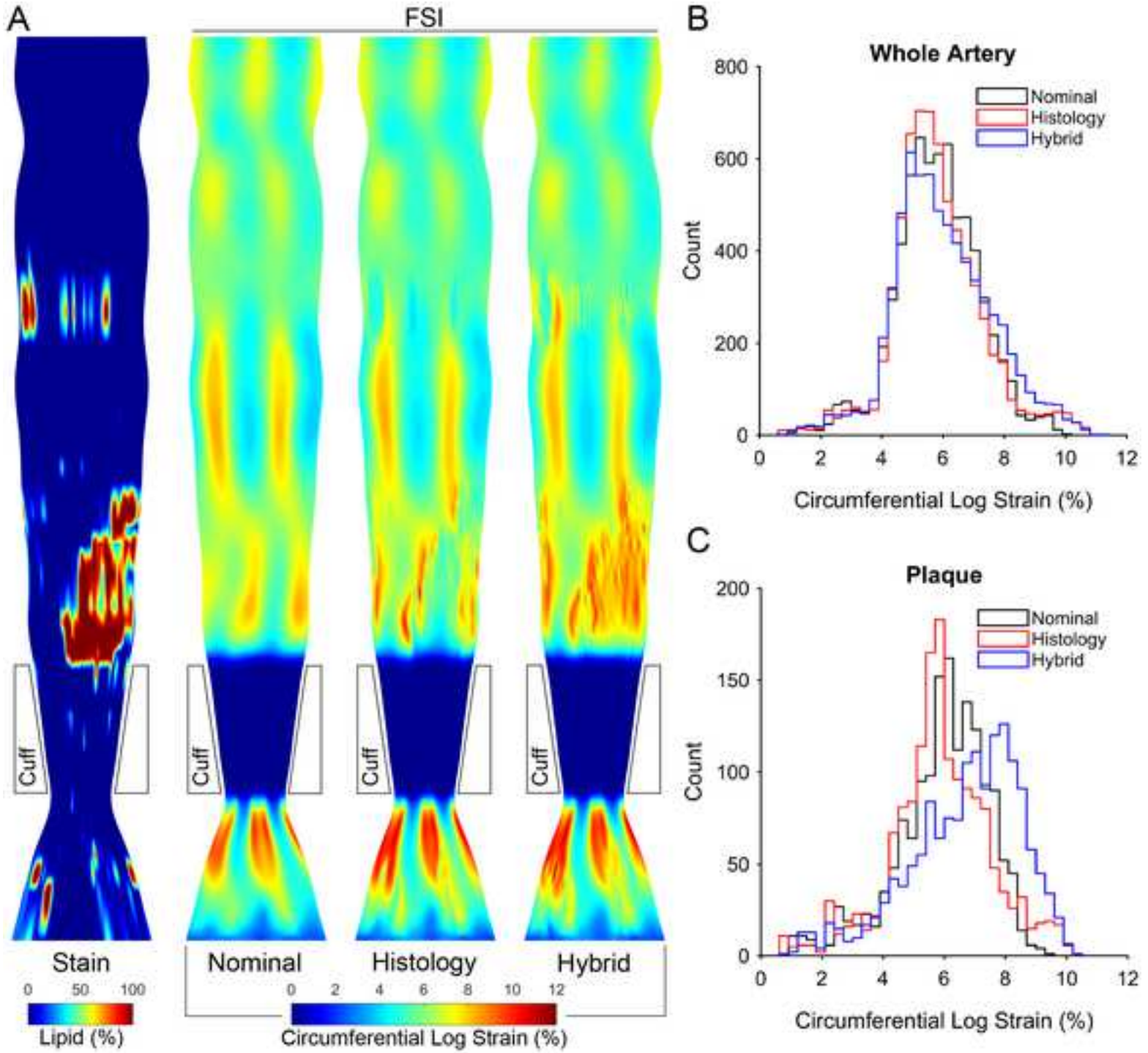

Figure

Click here to access/download;Figure;Fig5.tif

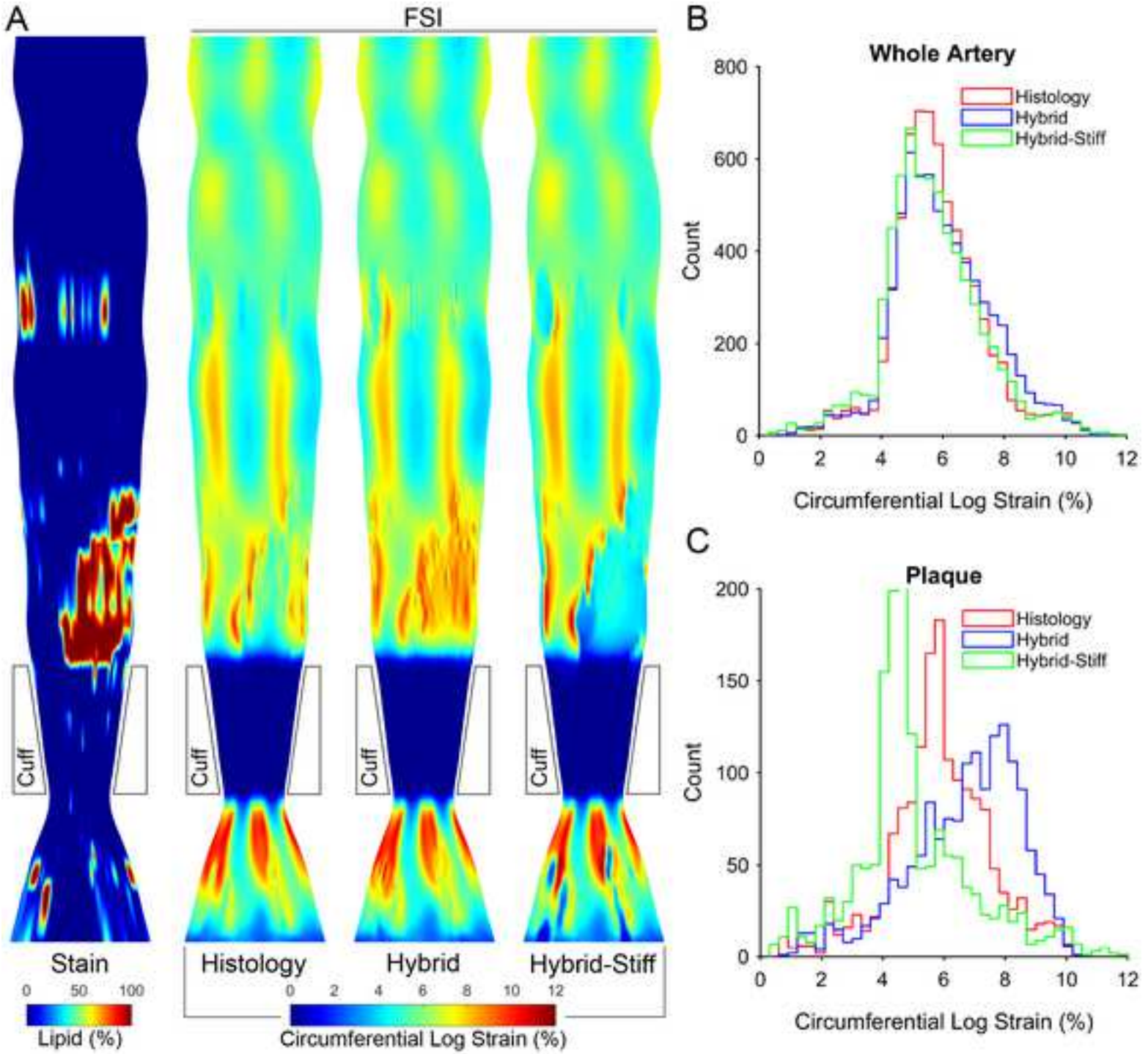

Figure

Click here to access/download;Figure;Fig6.tif

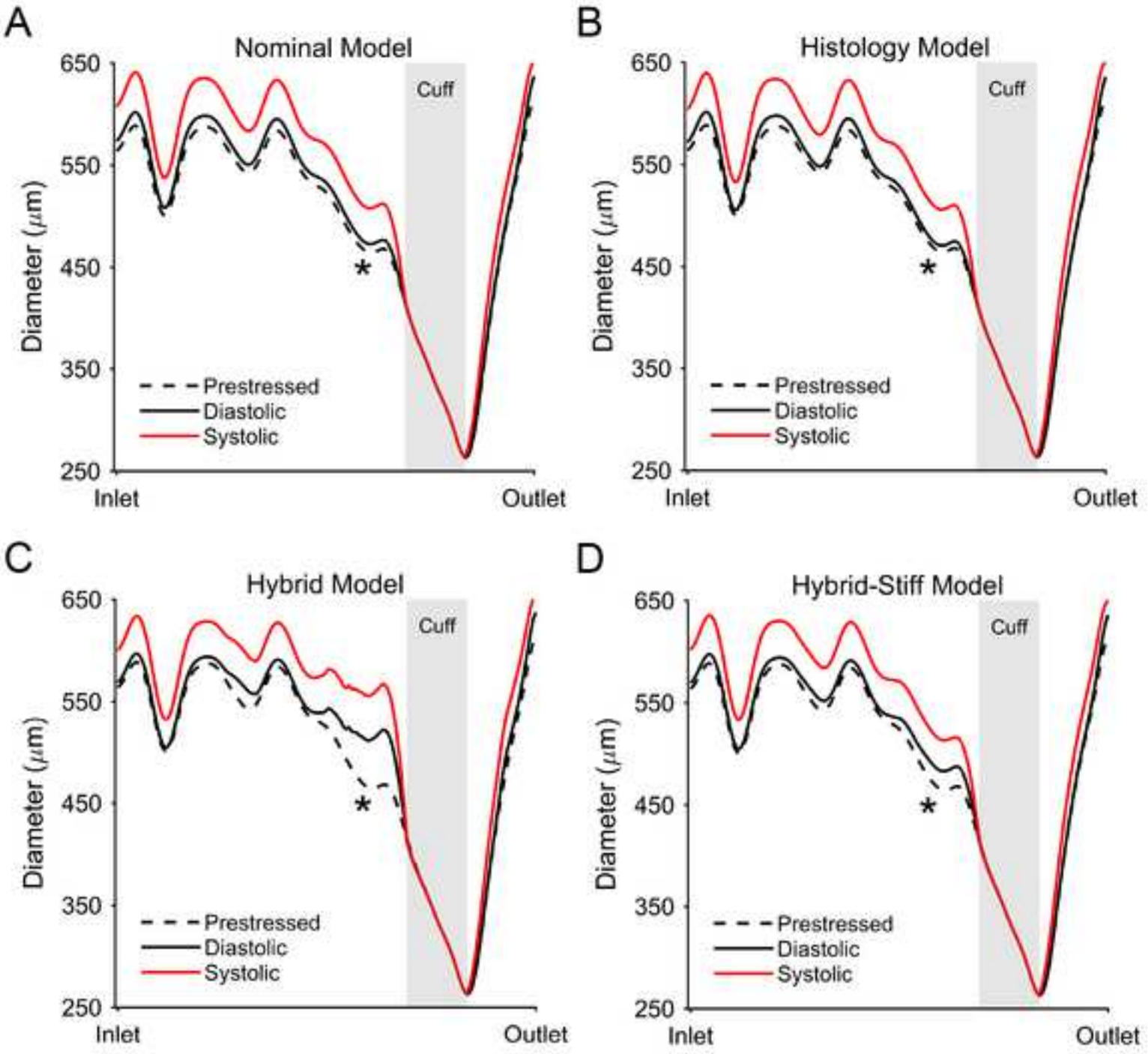

Figure

Click here to access/download;Figure;Fig7.tif

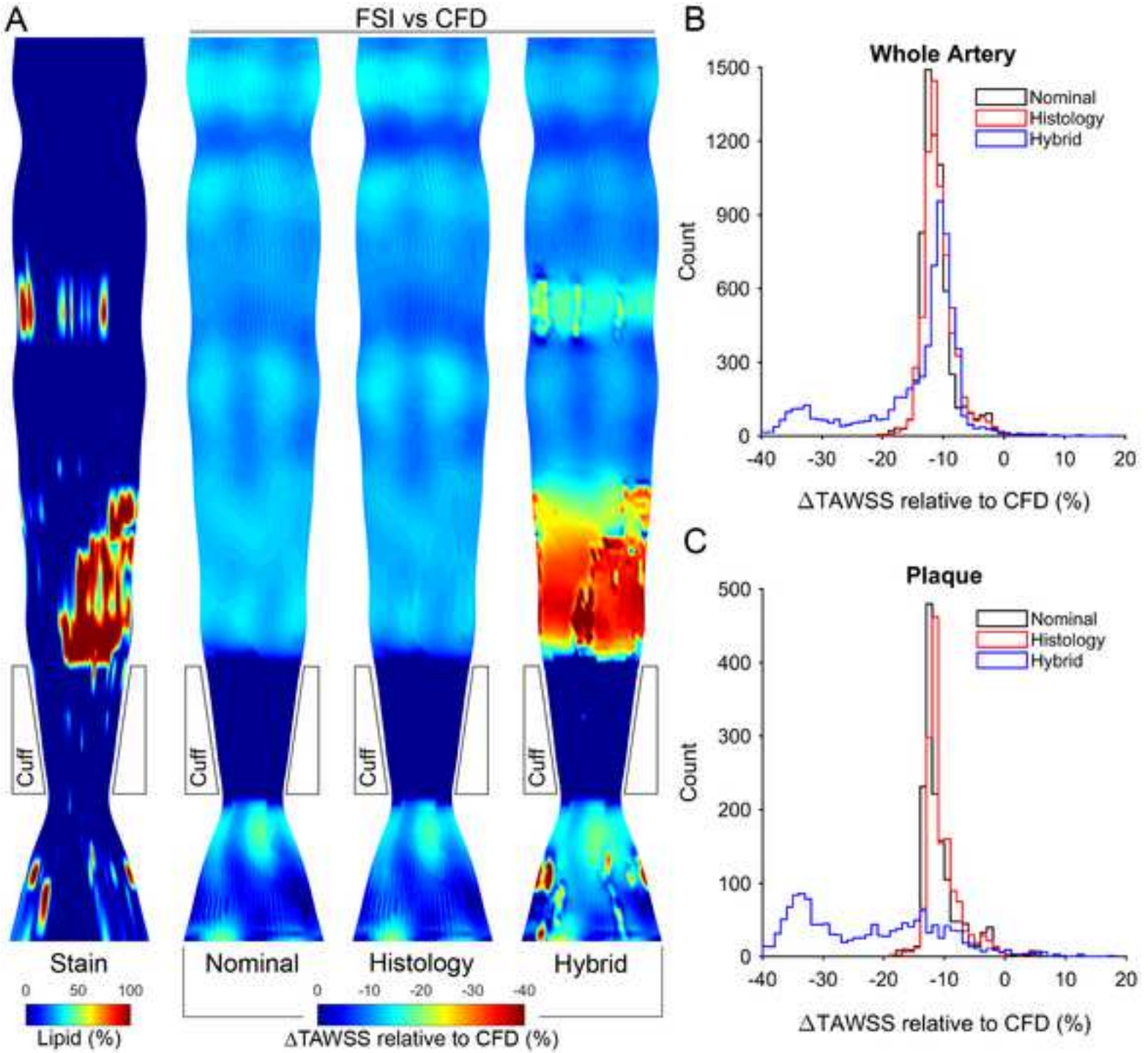

Considerations for analysis of endothelial shear stress and strain in FSI models of atherosclerosis

Appendix A. Supplementary material

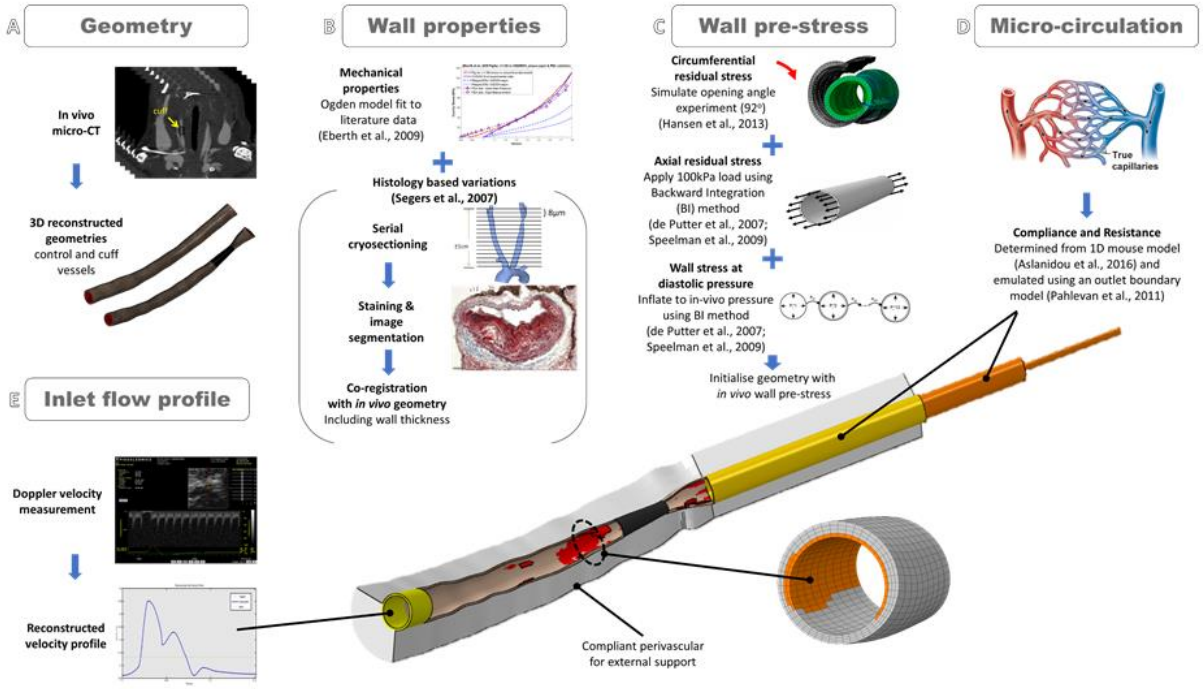

Fig. S1. Framework for developing the FSI models, including 3-D vessel reconstruction and incorporation of plaque heterogeneity from histology. (A) Lumen wall geometry is extracted from micro-CT and used to create an accurate 3D vessel geometry based lumen mesh. (B) Wall material properties fitted with an OGDEN model to data from the literature and assignment of softer properties to plaque areas based on percentage of lipid present. (C) FSI model initialised with diastolic in vivo vessel wall stress computed via solid-only opening angle closing, axial stretch and pressurization simulations. (D) Outlet boundary pressure waveform emulated using boundary model formulated based on typical compliance of murine cerebral vasculature. (E) Flow boundary conditions prescribed from Ultrasound flow velocity measurements at face of inlet extension.

Table S1: summary of constraints applied for the different simulation models employed.

Type	Location	Boundary Condition
Geometry	Inlet	Inlet extended by an extension (1.5*diameter in length) to facilitate flow profile to match lumen geometry
	Elastic outlet extension	Length and elasticity set to model compliance of downstream vasculature estimated to be 2.5E-14 m^4s^2/kg
	Rigid section with constraint at model outlet	Model the resistance of the downstream vasculature, optimised to produce diastole 80mmHg pressure in the vessel segment of interest
Static	Vessel Inlet	Allowed to dilate radially, constrained axially
	Vessel Outlet	Allowed to dilate radially, constrained axially
	Rigid Section	No movement permitted
	Outer surface of perivascular support	No movement permitted
	Vessel wall - Cuff model only	No movement is permitted in the area of the outer vessel wall in the cuff location in the cuff vessel models (Nominal, Histology, Hybrid, Hybrid-Stiff)
Dynamic	Lumen Inlet	Flow velocity waveform over the cardiac cycle based on ultrasound measurements with an idealised parabolic
	Lumen outlet (at end of model region)	Pressure of 10.5 mmHg representing venous pressure
	Vessel wall layers	Circumferential residual stress determined from angle closing and prestresses due to axial pre-stretch and diastolic blood pressure via the Backward Incremental method

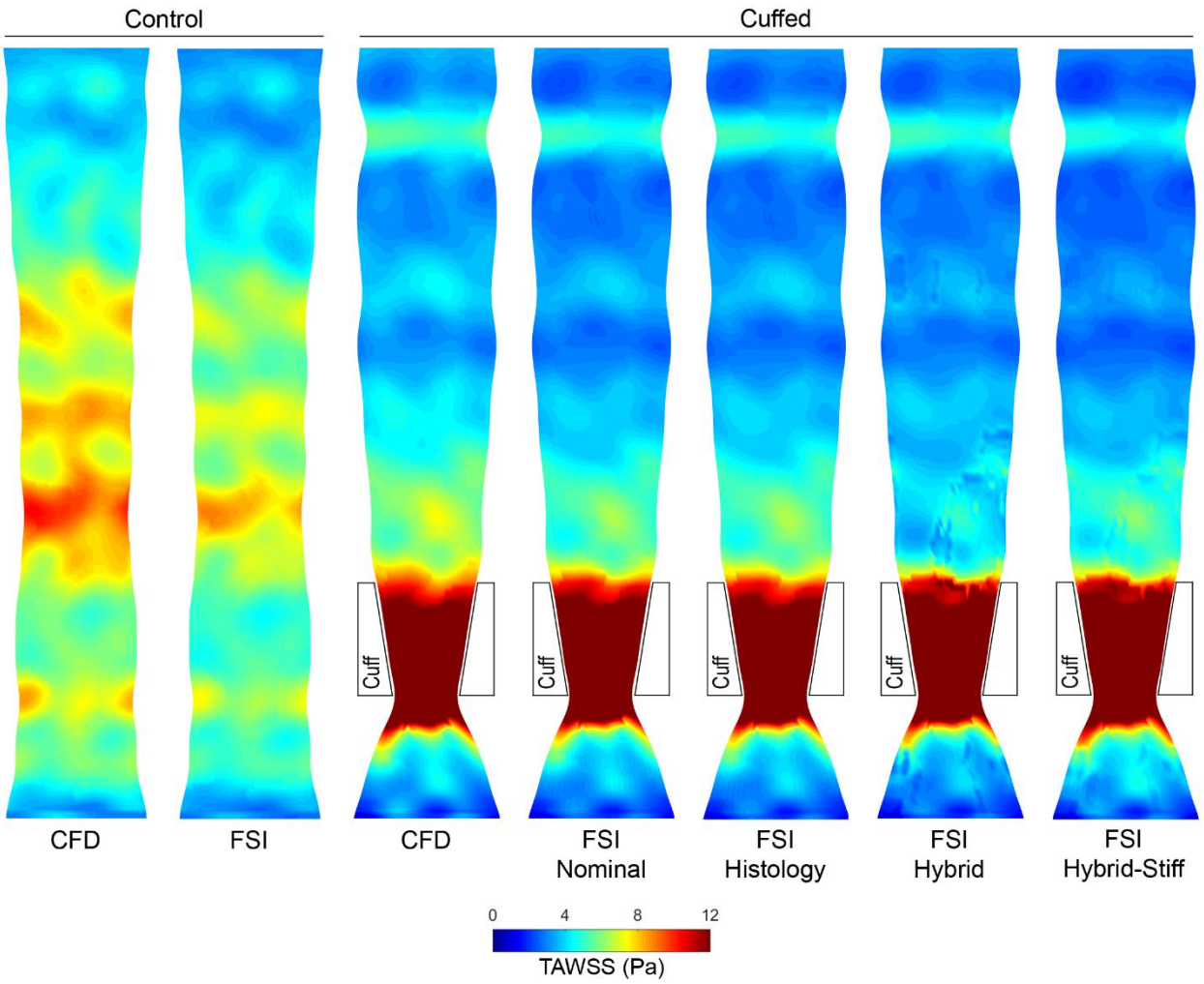

Fig. S2. The absolute magnitude of TAWSS for every model analyzed in this study, including: CFD control and cuff, and FSI control, Nominal, Histology, Hybrid, and Hybrid-Stiff models.

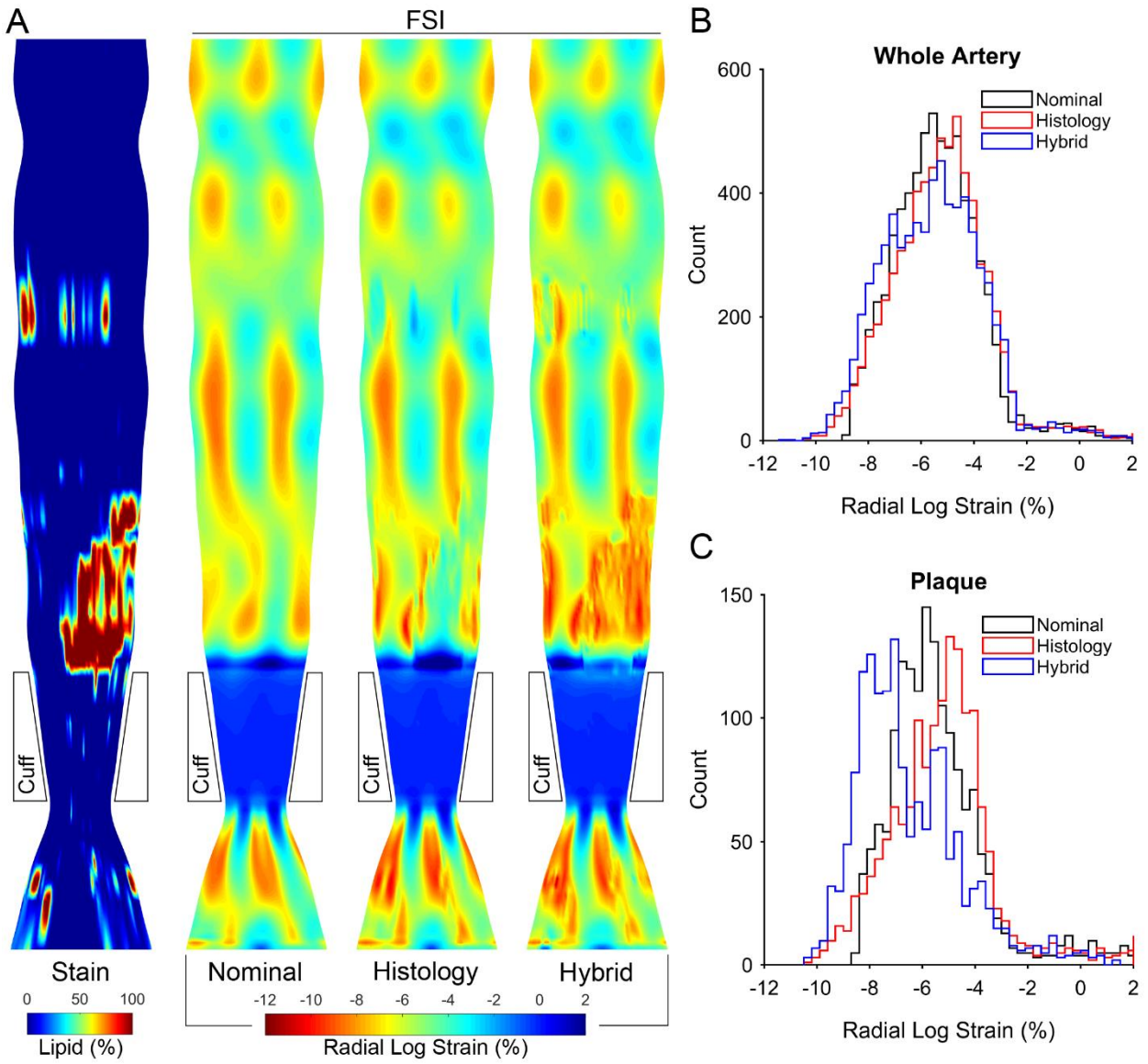

Fig. S3. Cyclic radial logarithmic strain (%) from FSI simulations of the Nominal Model, Histology Model, and Hybrid Model. In (A) 2D projections of the 3D histology (Oil Red O as reference) and of the 3D cyclic radial logarithmic strain are displayed from a single carotid artery obtained from the aortic arch (top) to just before the carotid bifurcation (bottom). The histological map shows the distribution of oil red O (lipid) staining and radial logarithmic strain (%) from the FSI simulations. (B-C) Histograms of the number of elements (count) for each increment of radial logarithmic strain (0.3%) in FSI (B) over the whole artery (excluding the cuff area) and (C) only in regions of lipid deposition (plaque) for each of the three models.

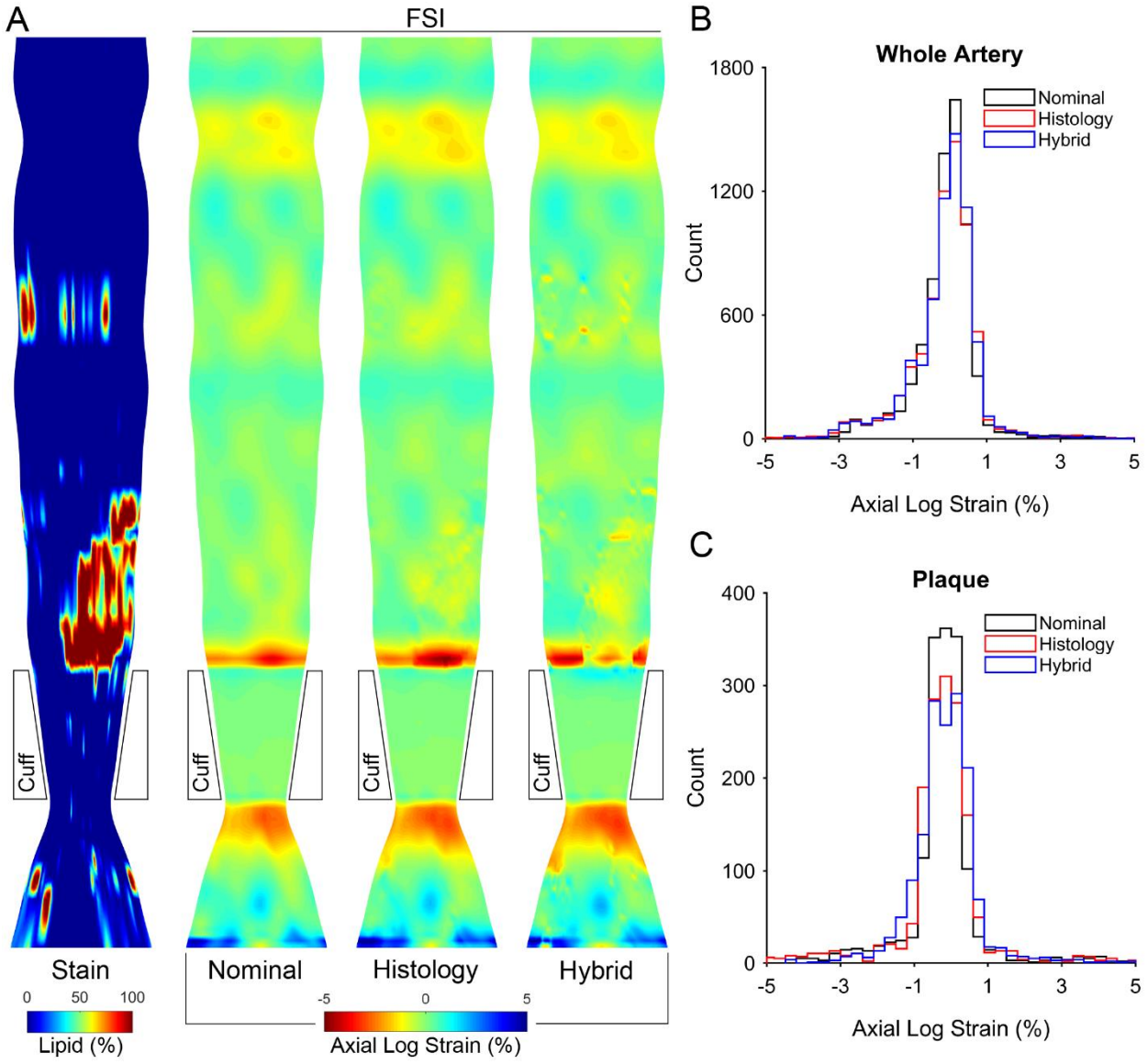

Fig. S4. Cyclic axial logarithmic strain (%) from FSI simulations of the Nominal Model, Histology Model, and Hybrid Model. In (A) 2D projections of the 3D histology (Oil-Red O as reference) and the 3D cyclic axial logarithmic strains are displayed from a single carotid artery obtained from the aortic arch (top) to just before the carotid bifurcation (bottom). (B-C) Histograms of the number of elements (count) for each increment of axial logarithmic strain (0.3%) in FSI (B) over the whole artery (excluding the cuff area) and (C) only in regions of lipid deposition (plaque) for each of the three models.

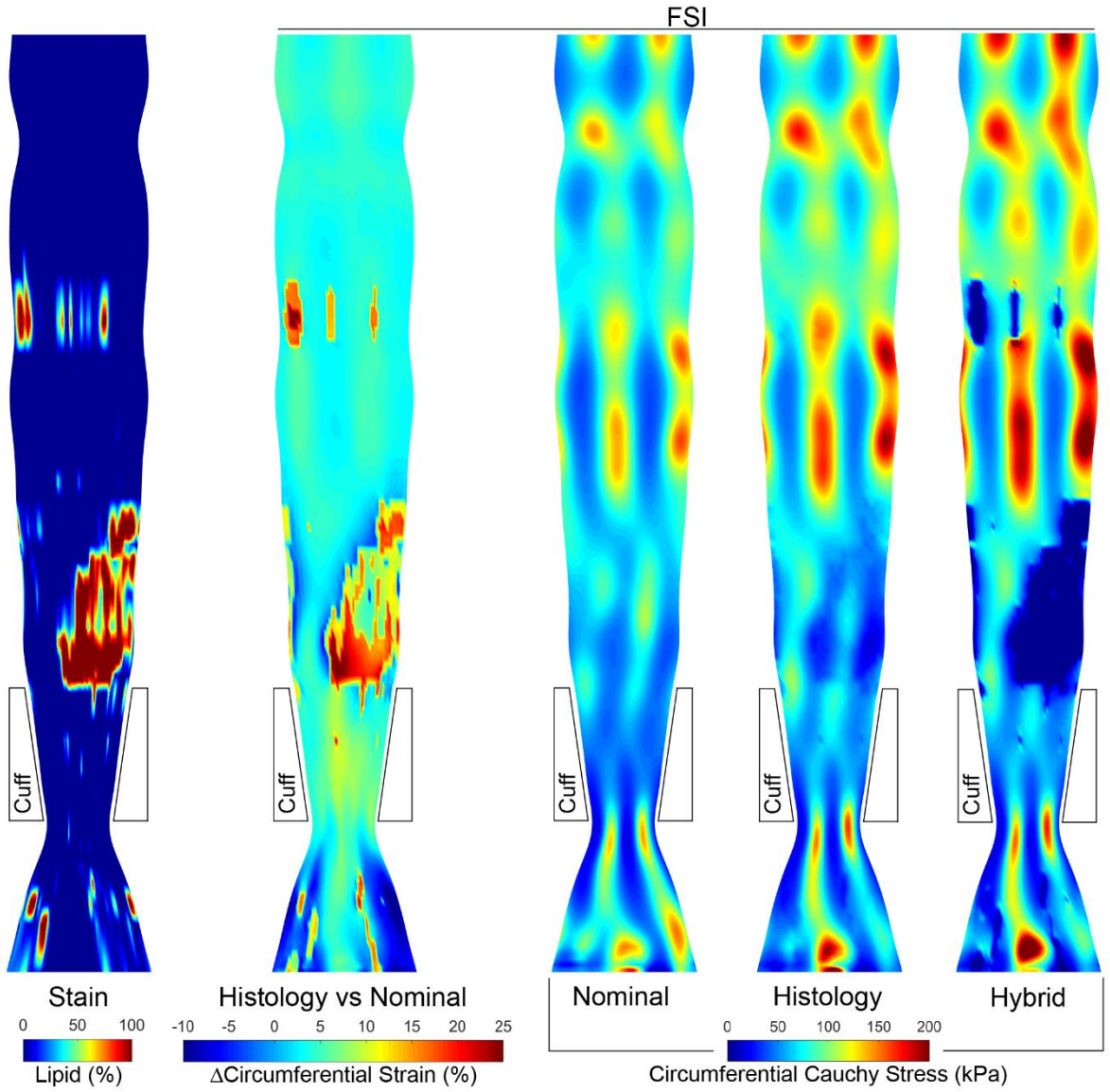

Fig. S5. As application of uniform pre-stresses did not produce satisfactory results, we propose a hybrid model (see text for further details). Difference in pre-stress circumferential logarithmic strain (Δ circumferential strain (%)) between FSI simulations of the Histology Model versus Nominal Model. Large differences only appear in regions of lipid deposition, where the softer properties in the Histology Model cause higher strains. Because of the nonlinear properties of the lipid, this results in a comparable prestress to that found at the same locations in the Nominal Model, indicating a similar stiffness. In the Hybrid Model, prestresses are set to zero before the start of the FSI simulation.

I hereby declare that none of the authors have a conflict of interest.

Professor Rob Krams